P.28

NASA TECHNICAL MEMORANDUM 107649

THERMAL RESIDUAL STRESSES IN SILICON-CARBIDE/TITANIUM [0/90] LAMINATE

C. A. Bigelow

JULY 1992

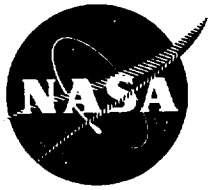

National Aeronautics and
Space Administration
Langley Research Center
Hampton, Virginia 23665-5225

THERMAL RESIDUAL STRESSES IN A SILICON-CARBIDE/TITANIUM [0/90] LAMINATE

C. A. Bigelow

ABSTRACT: The current work formulated a micromechanical analysis of a cross-ply laminate and calculated the thermal residual stress in a very thick $[0/90]_{2n}$ silicon-carbide/titanium laminate. Results were also shown for a unidirectional laminate of the same material. Discrete fiber-matrix models assuming a rectangular array of fibers with a fiber volume fraction of 32.5% and a three-dimensional, finite-element analysis were used. Significant differences in the trends and magnitudes for the fiber, matrix, and interface stresses were calculted for the unidirectional and [0/90] models. Larger hoop stresses calculated for the [0/90] model indicate that it may be more susceptible to radial cracking when subjected to mechanical loading than the unidirectional model. The axial stresses in the matrix were calculated to be slightly larger for the [0/90] model. The compressive axial stresses in the fiber were significantly larger in the [0/90] model. The presence of the cross-ply in the [0/90] model reduced the constraint on the fiber, producing radial interface stresses that were less compressive, which could lead to earlier failure of the fiber-matrix interface.

INTRODUCTION

Metal matrix composites have several inherent properties, such as high stiffness-to-weight ratios and high strength-to-weight ratios, which make them attractive for advanced aerospace applications. These composites also have a higher operating temperature range than current polymer matrix composites. However, the large differences that can occur in the coefficients of thermal expansion of the fiber and the matrix, combined with the large temperature change during fabrication, can lead to problems in these materials. High residual stresses can develop in the composite during cooldown from the fabrication temperature. The resulting stresses may be large enough to produce matrix cracks and interfacial debonding or plastically deform a ductile matrix. Thus, it is important to quantify these thermal residual stresses to understand their effects on the composite behavior.

Several analyses (e.g., [1-3]) have been done using the unit cell micromchanical model to calculate thermal residual stresses in unidirectional composites. The current work extends the micromechanical analysis to a cross-ply laminate. This paper analyzes the thermal residual stresses in a very thick $[0/90]_{2n}$ silicon-car-

bide/titanium laminate. A three-dimensional finite element analysis was conducted using temperature-dependent properties for both the fiber and matrix. For comparison, results are also shown for a unidirectional laminate of the same material with the same fiber volume fraction. Matrix stresses, fiber stresses, and interfacial stresses due to the temperature change during the fabrication cycle are calculated. The effects of matrix plasticity are investigated.

FINITE ELEMENT MODEL AND LOADING

For both laminates, a discrete fiber-matrix model assuming an infinitely repeating, rectangular array of fibers was used. MSC/NASTRAN [4], using three dimensional, eight-noded hexahedral elements, was used for the finite element analysis. The ply thickness (0.194 mm), the fiber volume fraction (32.5%), and the fiber diameter (0.140 mm) were used to calculate the dimensions of the models. The ply thickness, the fiber volume fraction, and the fiber diameter are typical for silicon-carbide/titanium composites and were taken from [5]. The particular metal matrix composite used herein is SCS-6/Ti-15-3, where Ti-15-3 is a shortened designation for Ti-15V-3Cr-3Al-3Sn and the manufacturer's designation for the silicon-carbide fibers is SCS-6. Ti-15-3 is currently under evaluation as a matrix material for high temperature metal matrix composites since is can be economically cold-formed into relatively thin sheets while retaining good mechanical properties [6].

Figures 1 and 2 show the finite element models that were used for the unidirectional and [0/90] models, respectively. A convergence study was done on the mesh used for the unidirectional model. For the thermal loading used here, the mesh shown in Figure 1 produced stresses that differed by less than 5% from those for a mesh with twice the refinement. Compatibility with adjacent unit cells was enforced by constraining the normal displacements of all nodes on each face to be equal. A perfect bond between the fiber and matrix was assumed in all analyses. The interphase was not modeled as a separate constituent since material properties are not available for the interphase region.

Thermal residual stresses were calculated assuming a temperature change of -538°C; the temperature 538°C is approximately one half of the melting point of the Ti-15-3 matrix. It was assumed that any residual stresses that developed during fabrication of the composite would be relieved due to relaxation at temperatures greater than one half the melting point of the matrix [7]. The temperature-dependent constituent properties [5] used are given in Table 1. The matrix properties are given for the as-fabricated material (i.e., no heat treatment). The matrix properties were determined from matrix specimens manufactured using the same foil material and processing cycle that were used for the composite. The tabulated data for the temperature-dependent matrix stress-strain curves are given in Table 2. The fiber was assumed to remain elastic with temperature-dependent properties.

RESULTS AND DISCUSSION

Matrix stresses, fiber stresses, and interface stresses are calculated for both the unidirectional and [0/90] laminates. All stresses are defined with respect to the cylindrical coordinate system shown in Figures 1 and 2. Within the [0/90] block, the fiber parallel to the z-axis is referred to as the 0^0 fiber and the fiber parallel to the x-axis is referred to as the 90^0 fiber. Stress results for the [0/90] model are presented for the 0^0 fiber and the matrix around the 0^0 fiber in the lower half of the model. Due to symmetry, the σ_{rr}, $\sigma_{\theta\theta}$, and σ_{zz} stresses are identical in either the top or bottom portion of the model with respect to a cylindrical coordinate system whose origin is located at the center of the fiber with the z-axis parallel to the fiber axial direction. The fiber in the unidirectional model is referred to as a 0^0 fiber. For clarity, stress contours are presented for the matrix only. Yielding of the matrix was determined by comparing the von Mises equivalent stress calculated at room temperature to the room temperature yield stress (689.5 MPa [5]). When the von Mises equivalent stress was greater than or equal to the yield stress, yielding of the matrix was assumed. The von Mises equivalent stress σ_{vm} is defined as follows:

$$\sigma_{vm} = \sqrt{\sigma_x^2 + \sigma_y^2 + \sigma_z^2 - \sigma_x\sigma_y - \sigma_y\sigma_z - \sigma_z\sigma_x + 3(\tau_{xy}^2 + \tau_{yz}^2 + \tau_{zx}^2)}$$

No yielding of the matrix was predicted during the fabrication process; thus, only results for the linear analyses are presented.

The three normal stress components, σ_{rr}, $\sigma_{\theta\theta}$, and σ_{zz}, can be related to different types of matrix damage in the form of cracking. The radial stress component σ_{rr} controls interfacial or circumferential cracking. The most common example of this type of cracking is fiber-matrix debonding. The hoop stress component $\sigma_{\theta\theta}$ controls radial cracking. The axial stress component σ_{zz} governs cracking perpendicular to the fiber direction.

Matrix Stresses

Radial. - The stress contours for the radial stress component for the unidirectional and [0/90] models are presented in Figures 3 and 4, respectively. The contour plots for the [0/90] composite (Fig. 4) are shown in two views of the model to show the stress distribution on all faces of the model. For the unidirectional model (Fig. 3), the σ_{rr} stress values range from a tensile value of 66 MPa to a compressive value of -250 MPa. For the [0/90] model (Fig. 4), the σ_{rr} stress values range from a tensile value of 132 MPa tensile to a compressive value of -289 MPa. The presence of the 0^0 fiber elevates the radial stresses, producing larger tensile and compressive values of the radial stress compared to the unidirectional case. The most obvious difference in the two calculations is in the z-direction, the axial fiber direction. The stresses are constant in the axial or z-direction for the unidirectional model, whereas there is considerable variation within the [0/90] model in the fiber

direction. The σ_{rr} stresses become larger as the back face (z = 0.0 mm) is approached (Figure 4(a)). The gradient in the radial stress is greater for the portion of the matrix where the 0° and 90° fibers are closest together (on the y-z plane). On the bottom face of the [0/90] model (the x-z plane, Figure 4(b)), the stresses are constant in the z-direction and vary uniformly with x. The radial stresses are tensile on the x = 0.123-mm plane in the [0/90] model (Fig 4(b)). On the x= 0.123-mm plane in the unidirectional model, the radial stress varies from a tensile value of 66 MPa to compressive value of -50 MPa. Since the radial stress component governs circumferential cracking in the matrix, the calculated stress distributions indicate a greater propensity for circumferential cracks to develop in the [0/90] laminate due to the thermal cycle and could also lead to earlier cracking when subjected to a mechanical loading after fabrication.

Hoop. - The stress contours for the hoop stress for the unidirectional and [0/90] models are given in Figures 5 and 6, respectively. The range of values and the general shape of the contours for the $\sigma_{\theta\theta}$ component are similar for the two models. In the unidirectional case, all values are tensile, ranging from 313 MPa to 68.3 MPa. In the [0/90] model, all values are tensile as well, ranging from 359 MPa to 108 MPa. In both cases, the maximum values occur in the matrix next to the fiber. For the unidirectional case, the maximum stresses are calculated over a large portion of the interface, from $\theta = 0°$ to 60°. As the radial distance from the fiber-matrix interface increases, the hoop stress decreases significantly. However, in the portion of the matrix above the fiber on the x = 0 plane, the hoop stress is nearly constant and, although not the maximum value, the stress in that area is a relatively high value, within 11% of the maximum hoop stress. In the [0/90] model, the stress contours on the front face (z = 0.123 mm) are very similar in shape to the contours for the unidirectional model, although the stress levels are 13% higher. In the [0/90] calculations, the hoop stress decreases as the radial distance from the fiber increases and also as one moves from the z = 0.123-mm plane to the z = 0.0-mm plane. In the unidirectional model, the minimum value is calculated at the top of the model, at approximately $\theta = 45°$. In the [0/90] model, the minimum value is also on the top surface of the model at the upper right corner of the back face (Fig. 6(a)). The larger hoop stresses calculated for the [0/90] model could lead to the initiation of radial cracking earlier in the loading compared to the unidirectional case, or, depending upon the matrix properties, radial cracking during the fabrication process. Such damage had been observed in unidirectional SCS-6/Ti-15-3 due to the thermal cooldown during the fabrication process [8].

Axial. - The presence of the 90° fiber produces considerable difference in the shape of the stress contours for the σ_{zz} stress component. The maximum and minimum stresses are similar for the unidirectional and [0/90] models (Figures 7 and 8, respectively), although the values are slightly greater for the [0/90] calculations. In the unidirectional case (Figure 7), the maximum σ_{zz} occurs near the fiber-matrix interface at $\theta = 45°$. In the [0/90] model, the maximum σ_{zz} occurs at

the upper corner of the back face of the model (Figure 8). As with the other stress components, there is significant variation in the σ_{zz} stress through the thickness of the [0/90] model.

Shear. - The only non-zero shear stress in the unidirectional model is the $\tau_{r\theta}$ component shown in Figure 9. The $\tau_{r\theta}$ stresses for the [0/90] model are presented in Figure 10. The magnitudes of the $\tau_{r\theta}$ shear stress components for both models are smaller than the other stress calculations. The shear stresses are of most interest on the fiber-matrix interface and, thus, will be discussed in detail in the later section on interface stresses.

Fiber Stresses

Since the coefficient of thermal expansion α for the matrix is more than twice as large as the coefficient of thermal expansion of the fiber (see Table 1), one would expect all the stresses in the fiber to be compressive. Indeed the analyses calculated all the fiber stresses to be compressive for both the unidirectional and [0/90] models; thus, no fiber damage would be expected due to the fabrication process. However, these stresses could act as a prestress that could affect the composite properties and subsequent mechanical behavior. For completeness the calculations of the radial, hoop, and axial components of the fiber stresses are discussed.

In the unidirectional case, the minimum value of radial stress σ_{rr} was at the edge of the fiber approximately at $\theta = 40^{\circ}$. In the [0/90] model, the minimum stress occurred along the fiber center line and extended nearly across the width of the fiber. For both the unidirectional and [0/90] cases, the minimum value of σ_{rr} was still a compressive stress, but the minimum for the [0/90] calculation was only 37% of that for the unidirectional. The stress distributions for the hoop stresses were similar for the two models and very similar to the radial component.

The axial stress component is of most concern in predicting fiber fracture. In the unidirectional calculations, the axial stress was nearly uniform throughout the model, with a variation of less than 2% across the fiber and an average value of -500 MPa. The magnitude of the axial stress was much larger than the radial or hoop stress. For the [0/90] calculation, the axial stress was not as uniform, it varied by 13% through the fiber, ranging from -660 MPa to -760 MPa. The magnitude of the fiber axial stress was much larger for the [0/90] calculations, by 24% to 34%. The axial stress calculations indicate that a greater mechanical axial load would be necessary in the [0/90] than in the unidirectional model to overcome the thermal residual stresses.

Matrix Stresses at the Interface

The interphase was not modeled as a separate constituent since material properties are not available for the interphase region. All interface stresses presented are the stresses in the matrix layer next to the fiber. As stated earlier, an

intact bond between the fiber and matrix is assumed in all results. The interface stresses for the unidirectional model are shown in Figure 11. The σ_{rr} component is compressive for all values of θ and the $\sigma_{\theta\theta}$ and σ_{zz} are tensile for all values of θ. These interface stresses will cause the matrix to grip the fiber, even if the fiber-matrix interface has debonded. This type of behavior has been observed experimentally in SCS-6/Ti-15-3 composites [5]. The interface stresses around the 90° fiber in the [0/90] block are shown in Figures 12 through 17. Since the interface stresses in the [0/90] model vary as a function of z, the stresses are plotted for various values of z along the length of the 0° fiber. For comparison, the stresses calculated for the unidirectional case are shown in each figure.

The radial components of the matrix stresses at the interface are presented in Figure 12. For the unidirectional case, the peak (minimum compressive value) occurred near $\theta = 45°$; for the [0/90] model, the peak for all values of z occurred at $\theta = 0°$. For both models the maximum compressive stress occurred at $\theta = 90°$. In the [0/90] model, $\theta = 90°$ is the location on the 0° fiber-matrix interface closest to the 90° fiber and $z = 0.0$ mm is the back face of the [0/90] model, i.e., the plane which intersects the center line of the 0° fiber. In the [0/90] model, the effect of the 90° fiber increases as the z-coordinate decreases. Thus, as the z-coordinate decreases, the maximum compressive value of σ_{rr} for the 0° fiber increases significantly; the minimum compressive value also increases, but only slightly. The presence of the 90° fiber reduced the constraining effect of the matrix surrounding the 0° fiber. The radial component of stress governs failure of the fiber-matrix interface. Since the compressive σ_{rr} stresses are reduced in the [0/90] model, compared to the unidirectional case, the fiber-matrix interface may debond earlier in the [0/90] laminate when subjected to mechanical loading.

The hoop components of the matrix stresses at the interface are presented in Figure 13. Similar to the radial component, the hoop stress increases as the z-coordinate increases, with a larger variation at $\theta = 90°$. The maximum hoop stresses calculated for the [0/90] model are 13% larger at $z = 0.123$ mm than those calculated for the unidirectional case. The interfacial hoop stress component governs radial cracking. The larger hoop stresses calculated for the [0/90] model could lead to the initiation of radial cracking earlier in the loading, or, depending upon the matrix properties, radial cracking during the fabrication process. Such damage had been observed in unidirectional SCS-6/Ti-15-3 due to the thermal cooldown during the fabrication process [8].

The axial stress components of the matrix stresses at the interface are shown in Figure 14. The magnitudes of the axial stress are nearly equal for both cases. However, the trends in the curves are different for the two cases. For the unidirectional case, the peak value occurs near $\theta = 45°$; whereas for the [0/90], the maximum value occurs at $\theta = 0°$. Also, in this thermal loading case, the maximum value

of axial stress calculated for the unidirectional is slightly greater, by 5%, than that calculated for the [0/90] model.

The $\tau_{r\theta}$ stress components of the matrix stresses at the interface are shown in Figure 15. For the $\tau_{r\theta}$ shear stress, the calculations for the unidirectional case and the [0/90] model are similar. The calculations for the [0/90] model are shifted slightly and flattened somewhat compared to the unidirectional calculations.

The $\tau_{\theta z}$ and τ_{zr} stress components of the matrix stresses at the interface for the [0/90] model are shown in Figures 16 and 17, respectively. These two shear stress components are zero for the unidirectional case. As seen in the figures, the magnitudes of these stresses are small compared to the other stress components. As with the other stress calculations, there is significant variation in the maximum values as the z-coordinate varies, with a smaller variation in the minimum value.

CONCLUDING REMARKS

The current work formulated a micromechanical analysis of a cross-ply laminate and calculated the thermal residual stresses in a very thick $[0/90]_{2n}$ SCS-6/Ti-15-3 laminate. Results were also shown for a unidirectional laminate of the same material. For both laminates, a discrete fiber-matrix model assuming a rectangular array of fibers with a fiber volume fraction of 32.5% was used. A three-dimensional finite element analysis was used. Significant differences in the trends and magnitudes for the fiber, matrix, and interface stresses were calculated for the unidirectional and [0/90] models. The larger hoop stress calculated for the [0/90] model indicate that it may be more susceptible to radial cracking when subjected to mechanical loading than the unidirectional model. The axial stresses in the matrix were calculated to be slightly larger for the [0/90] model. The compressive axial stresses in the fiber were significantly larger (24-34%) in the [0/90] model, compared to the unidirectional case. The presence of the cross-ply in the [0/90] model reduced the constraint on the fiber, resulting in radial interface stresses that were less compressive, which could lead to earlier failure of the fiber-matrix interface.

REFERENCES

1. Nimmer, R. P.: Fiber-Matrix Interface Effects in the Presence of Thermally Induced Residual Stresses. *Journal of Composites Technology & Research*, Vol. 12, No. 2, Summer 1990, pp. 65-75.

2. Wisnom, M. R.: Factors Affecting the Transverse Tensile Strength of Unidirectional Continuous Silicon Carbide Fibre Reinforced 6061 Aluminum. *Journal of Composite Materials*, Vol. 24, July 1990, pp. 707-726.

3. Naik, R. A.; Johnson, W. S.; and Dicus, D. L.: Micromechanical Thermal Analysis of Interphase Region in a Titanium Aluminide MMC. Presented at the Titanium Aluminide Metal-Matrix Composites Workshop, May 16-18, 1990, Orlando, FL.

4. MSC/NASTRAN, Version 6.6, MacNeal-Schwendler Corporation, 1991.

5. Johnson, W. S.; Lubowinski, S. J.; and Highsmith, A. L.: Mechanical Characterization of Unnotched SCS_6/Ti-15-3 Metal Matrix Composites at Room Temperature. *Thermal and Mechanical Behavior of Metal Matrix and Ceramic Matrix Composites, ASTM STP 1080*, J. M. Kennedy, H. H. Moeller, and W. S. Johnson, Eds., American Society for Testing and Materials, Philadelphia, 1990, pp. 193-218.

6. Rosenberg, H. W.: Ti-15-3 - A New Cold-Formable Sheet Titanium. *Journal of Metals*, Vol. 35, No. 11, Nov. 1986, pp. 30-34.

7. Dieter, G. E.: *Mechanical Metallurgy*. 2nd Ed., McGraw-Hill, New York, 1976, pp. 451-489.

8. MacKay, Rebecca A.: Effect of Fiber Spacing on Interfacial Damage in a Metal Matrix Composite. *Scripta METALLURGICA et MATERIALA*, Vol. 24, 1990, pp. 167-172.

Table 1 - Temperature-Dependent Constituent Properties For SCS-6/Ti-15-3

Elastic Properties of Ti-15-3 Matrix (as-fabricated)

Temp (°C)	E (Pa)	ν	α (mm/mm/°C)
21.111	9.239E10	.36	8.208E-6
204.44	9.239E10	.36	8.946E-6
426.67	8.481E10	.36	9.504E-6
537.78	5.861E10	.36	9.756E-6

Elastic Properties of SCS-6 Fiber

Temp (°C)	E (Pa)	ν	α (mm/mm/°C)
21.111	3.93E11	.25	3.564E-6
93.333	3.90E11	.25	3.564E-6
204.44	3.86E11	.25	3.618E-6
315.56	3.82E11	.25	3.726E-6
426.67	3.78E11	.25	3.906E-6
537.78	3.74E11	.25	4.068E-6
648.89	3.70E11	.25	4.266E-6
760.00	3.65E11	.25	4.410E-6
871.11	3.61E11	.25	4.572E-6
1093.3	3.54E11	.25	

Tabulated Data for Ti-15-3 Matrix Stress-Strain Curves (as-fabricated)

Temp (°C)	Strain	Stress (Pa)
21.11	0.0	0.0
	0.0076	6.8948E8
	0.0082	7.4119E8
	0.0088	7.8428E8
	0.0094	8.2737E8
	0.0098	8.4461E8
	0.0106	8.7908E8
	0.0113	8.9632E8
	0.0118	9.0494E8
	0.0124	9.1356E8
	0.0132	9.2217E8
	0.0146	9.3079E8
	0.0168	9.3941E8
	0.0208	9.4803E8
537.78	0.0	0.0
	0.0071	4.1385E8
	0.0171	4.4816E8
	0.0321	5.0000E8

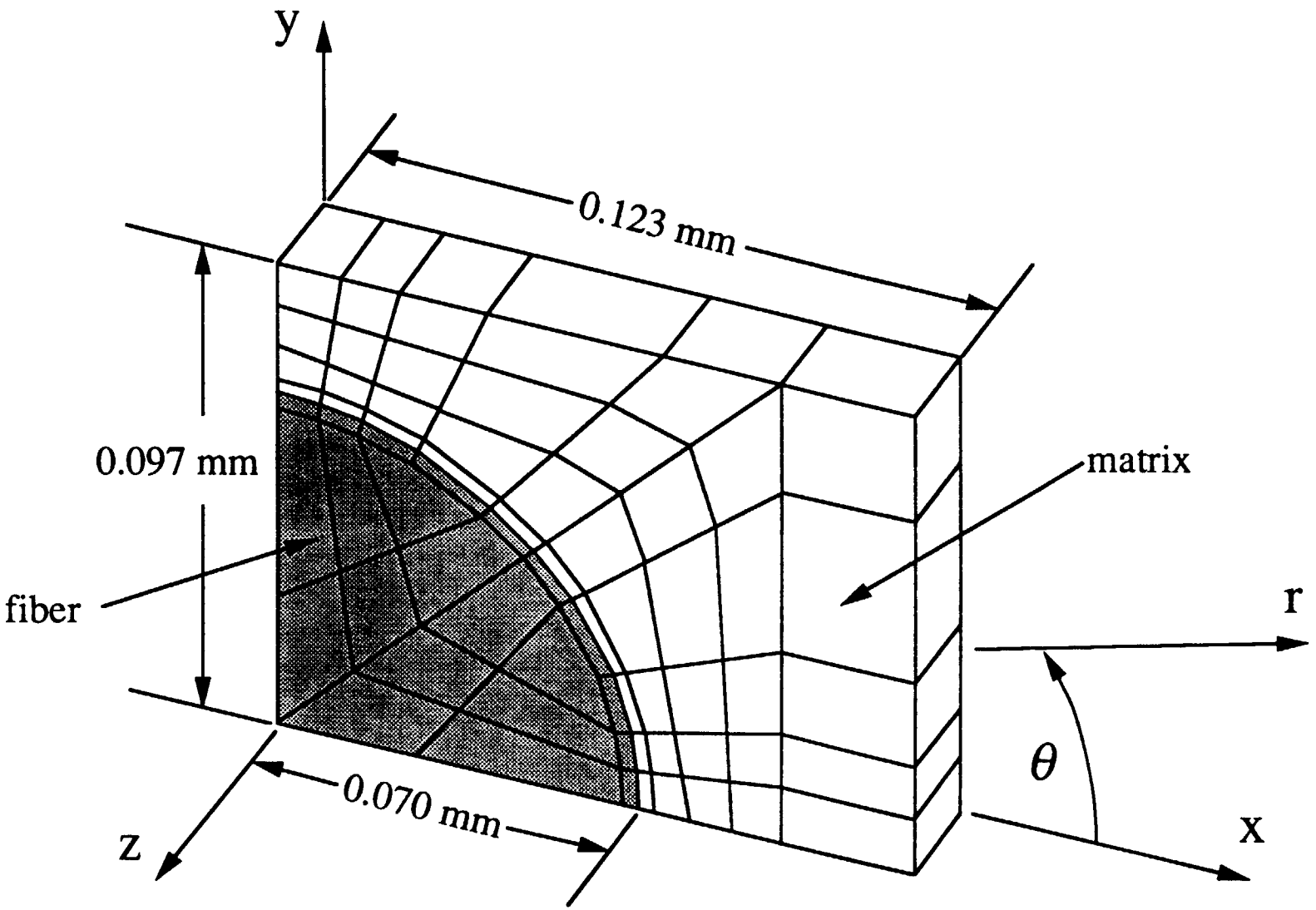

Figure 1. - Finite element mesh and dimensions for unidirectional unit cell. $v_f = 32.5\%$.

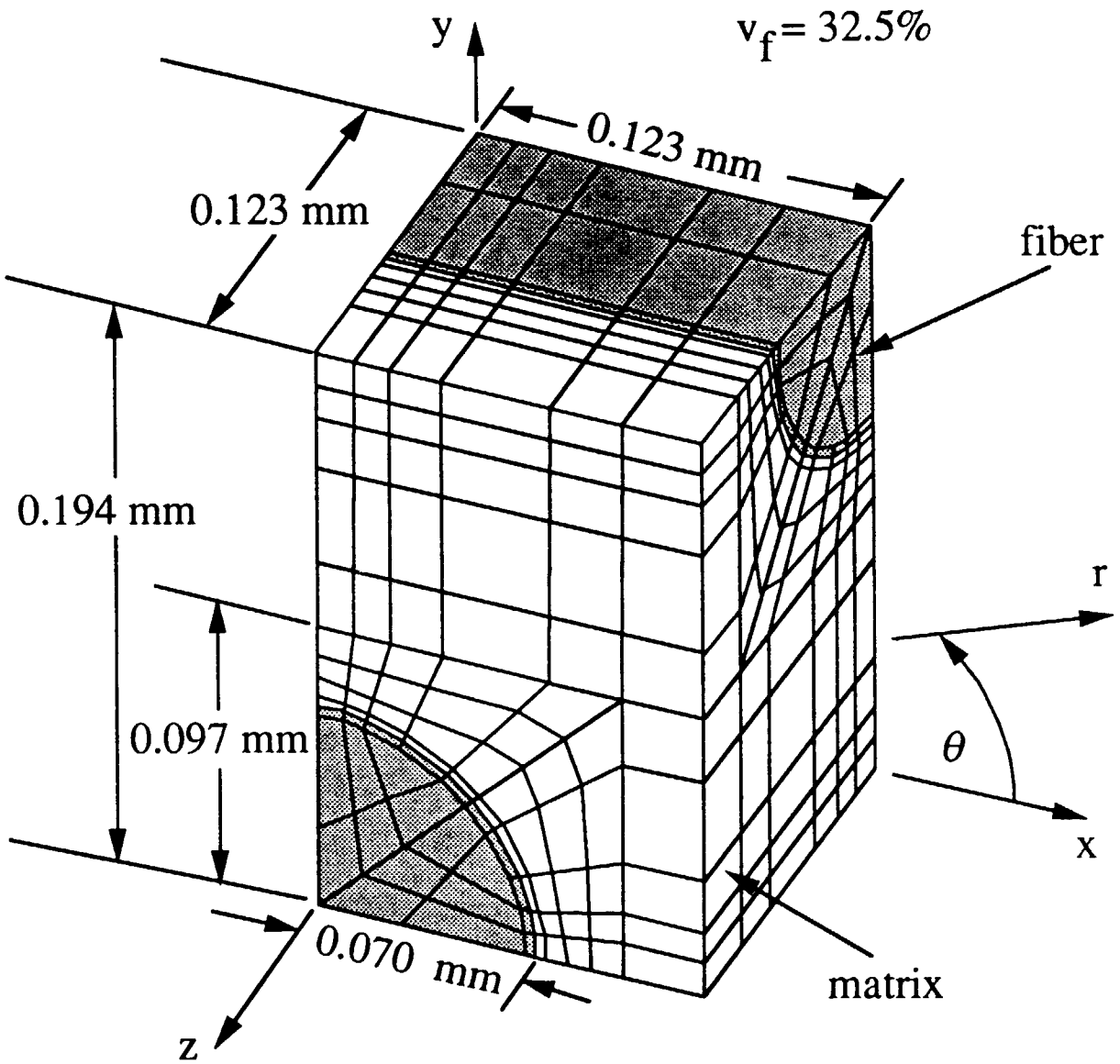

Figure 2. - Finite element mesh and dimensions for [0/90] model. v_f = 32.5%.

Level	Stress (MPa)
A	66.0
B	43.3
C	20.8
D	-1.8
E	-24.4
F	-47.0
G	-69.6
H	-92.2
I	-115
J	-137
K	-160
L	-183
M	-205
N	-228
O	-250

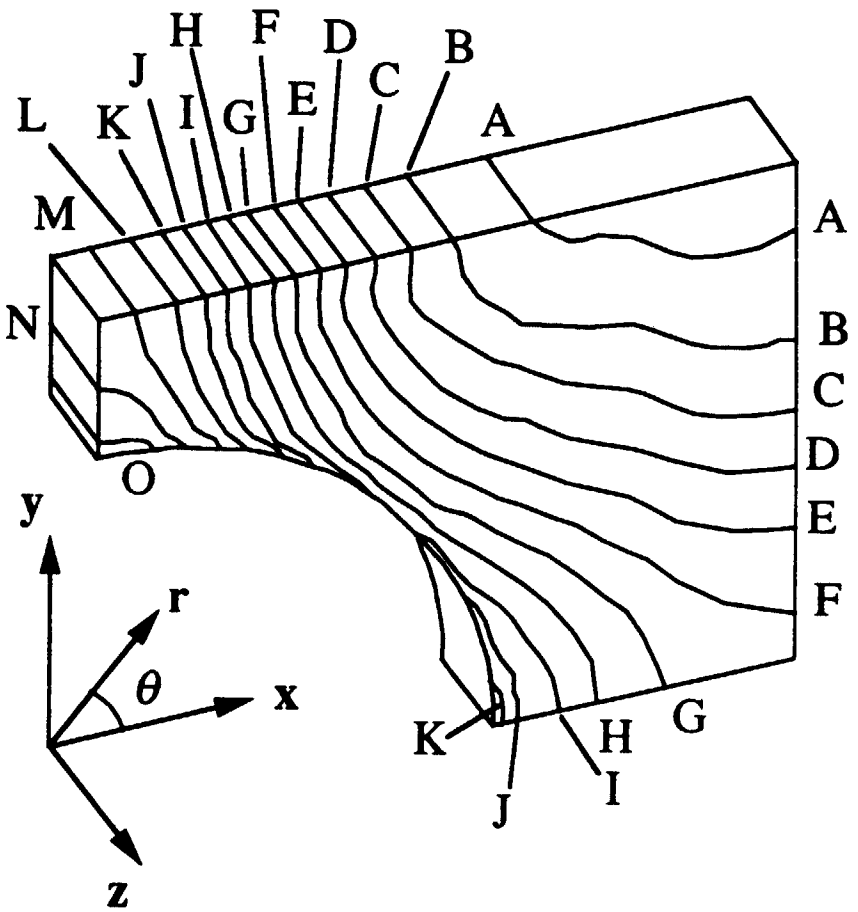

Figure 3. - Matrix σ_{rr} stress contours for unidirectional SCS-6/Ti-15-3, v_f = 32.5%, ΔT = -538°C

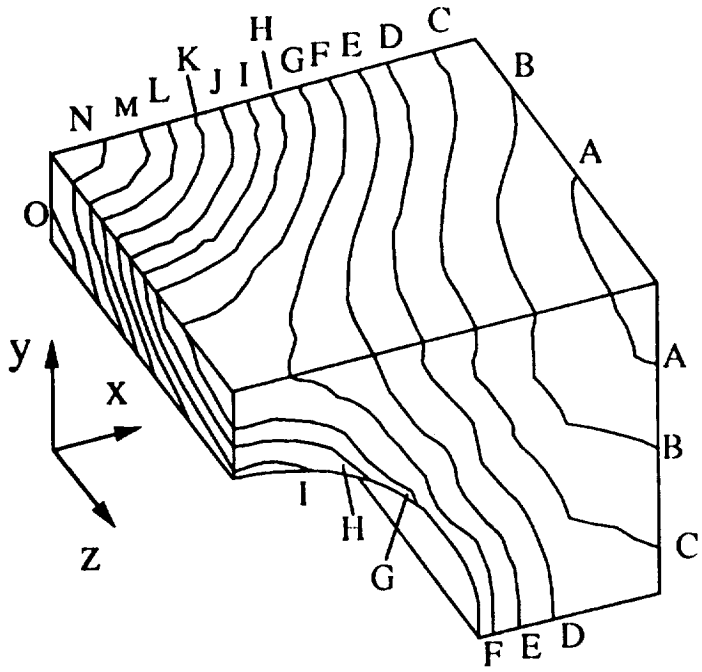

Level	Stress (MPa)
A	133
B	103
C	72.5
D	42.4
E	12.2
F	-17.9
G	-48.0
H	-78.1
I	-108
J	-138
K	-169
L	-199
M	-229
N	-259
O	-299

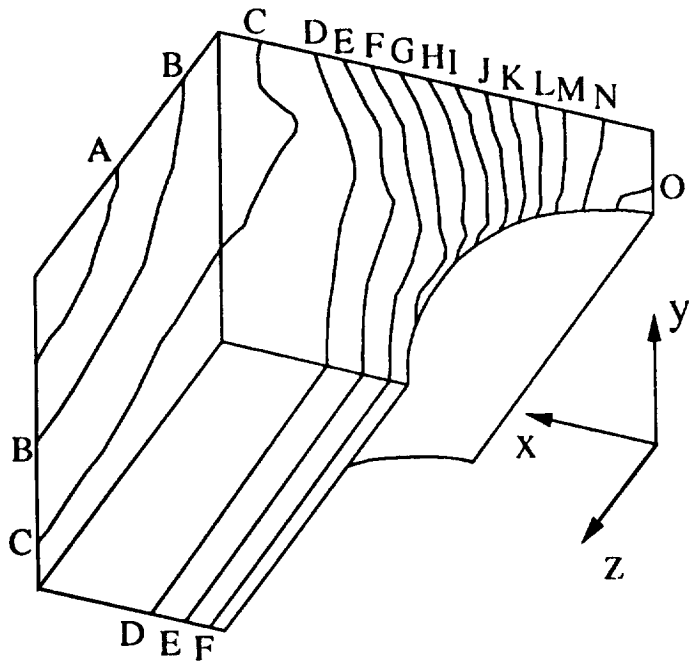

Figure 4. - Matrix σ_{rr} stress contours for [0/90] SCS-6/Ti-15-3, v_f = 32.5%, ΔT = -538°C.

Level	Stress (MPa)
A	312
B	295
C	278
D	260
E	243
F	225
G	208
H	190
I	173
J	156
K	138
L	121
M	103
N	86
O	68

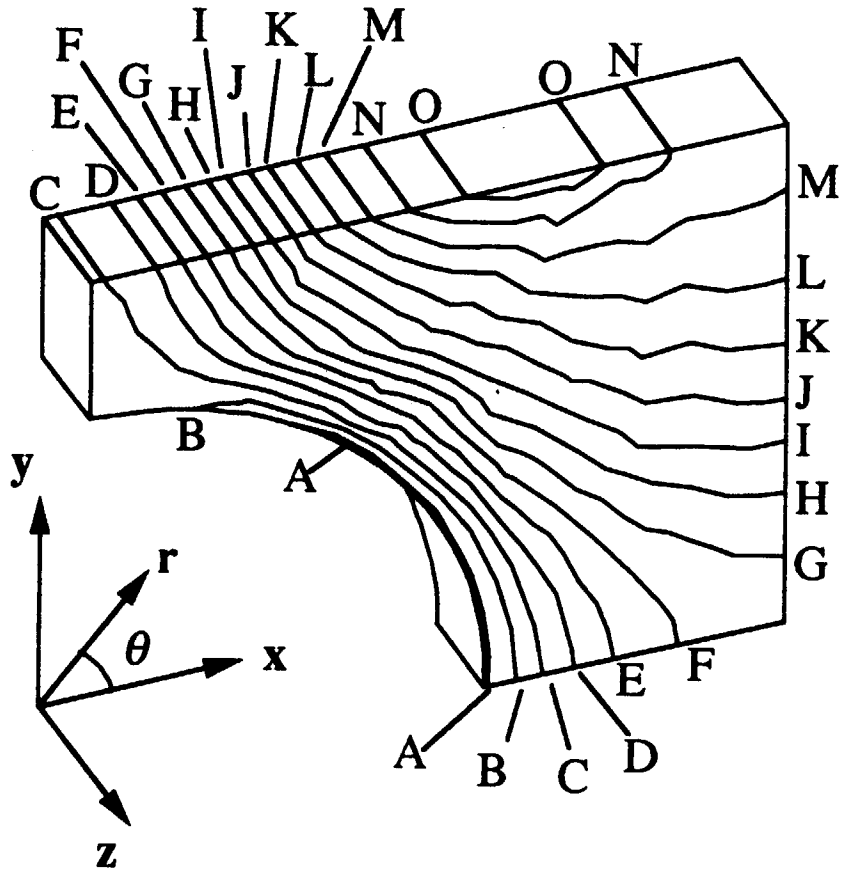

Figure 5. - Matrix $\sigma_{\theta\theta}$ stress contours for unidirectional SCS-6/Ti-15-3, $v_f = 32.5\%$, $\Delta T = -538°C$.

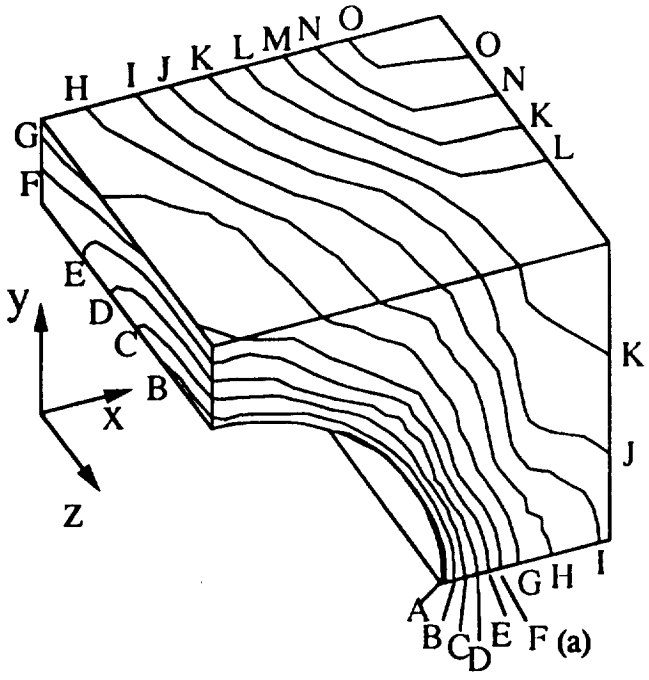

Level	Stress (MPa)
A	359
B	341
C	323
D	305
E	287
F	269
G	251
H	233
I	215
J	197
K	179
L	163
M	144
N	126
O	108

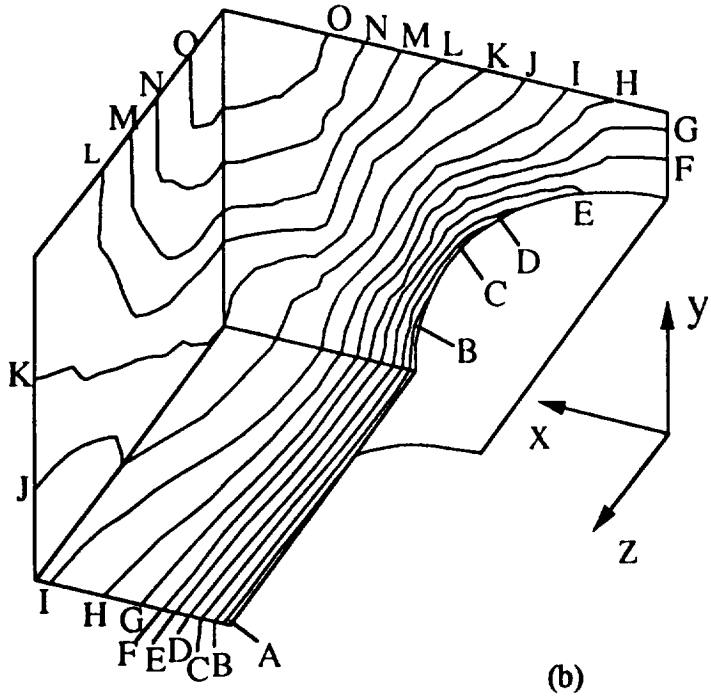

Figure 6. - Matrix $\sigma_{\theta\theta}$ stress contours for [0/90] SCS-6/Ti-15-3, v_f = 32.5%, ΔT = -538°C.

Level	Stress (MPa)
A	257
B	253
C	248
D	244
E	240
F	235
G	231
H	226
I	222
J	217
K	213
L	208
M	204
N	199
O	195

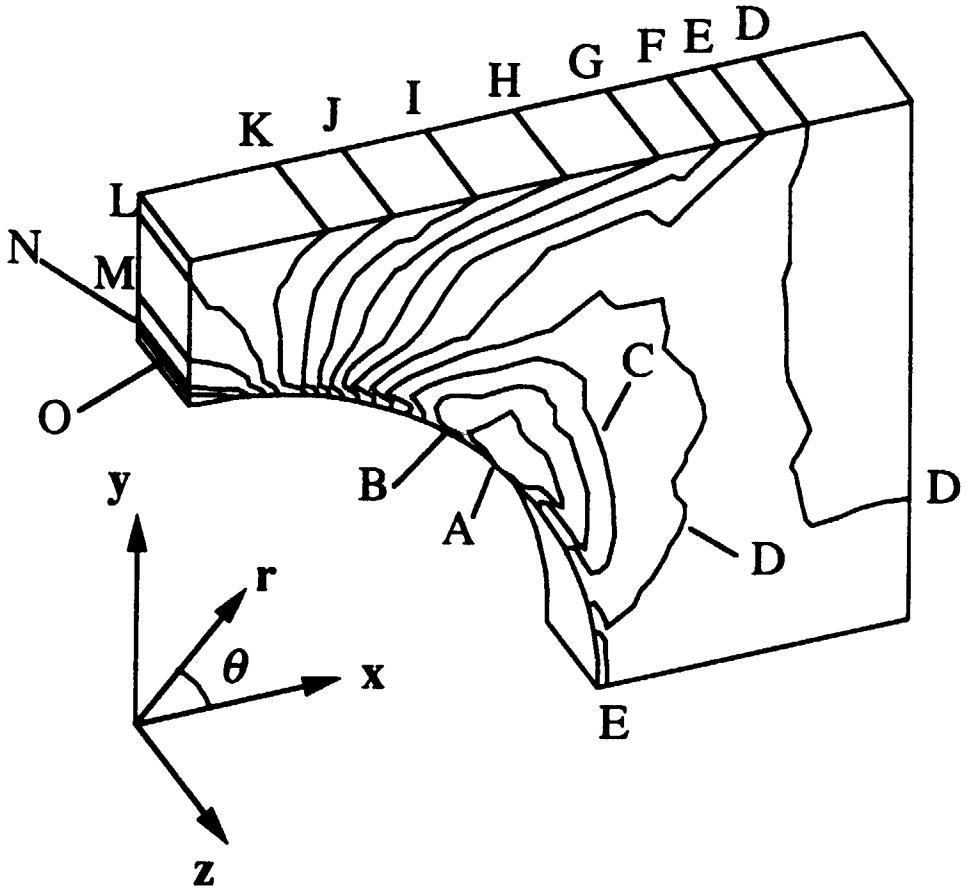

Figure 7. - Matrix σ_{zz} stress contours for unidirectional SCS-6/Ti-15-3, v_f = 32.5%, ΔT = -538°C.

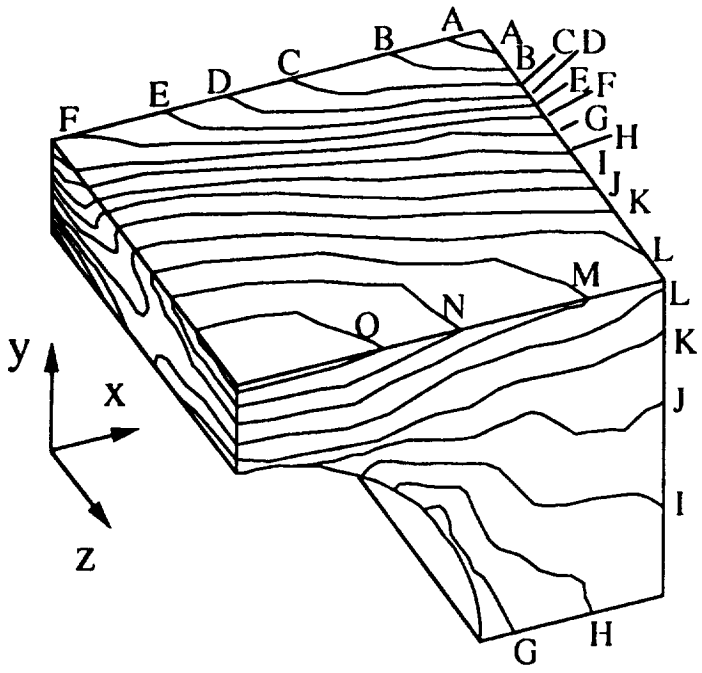

(a)

Level	Stress (MPa)
A	295
B	284
C	274
D	263
E	252
F	241
G	230
H	219
I	208
J	197
K	186
L	176
M	165
N	154
O	143

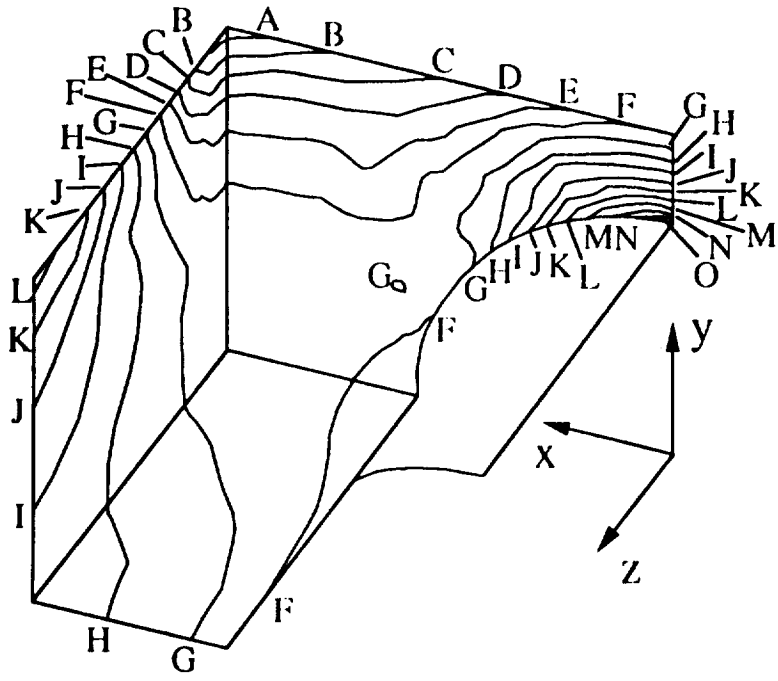

(b)

Figure 8. - Matrix σ_{zz} stress contours for [0/90] SCS-6/Ti-15-3, v_f = 32.5%, ΔT = -538°C.

Level	Stress (MPa)
A	45.5
B	36.7
C	27.9
D	19.1
E	10.3
F	1.5
G	-7.3
H	-16.1
I	-24.9
J	-33.7
K	-42.5
L	-51.3
M	-60.1
N	-68.9
O	-77.7

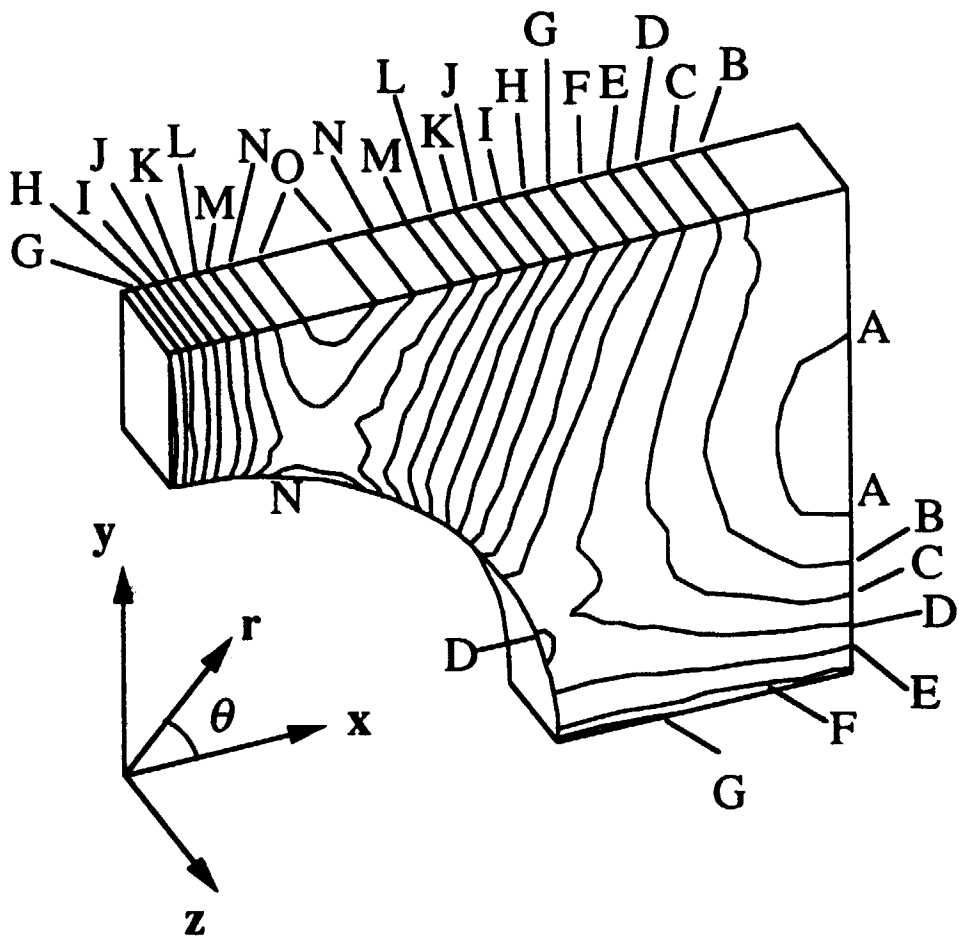

Figure 9. - Matrix $\tau_{r\theta}$ stress contours for unidirectional SCS-6/Ti-15-3, v_f = 32.5%, ΔT = -538°C.

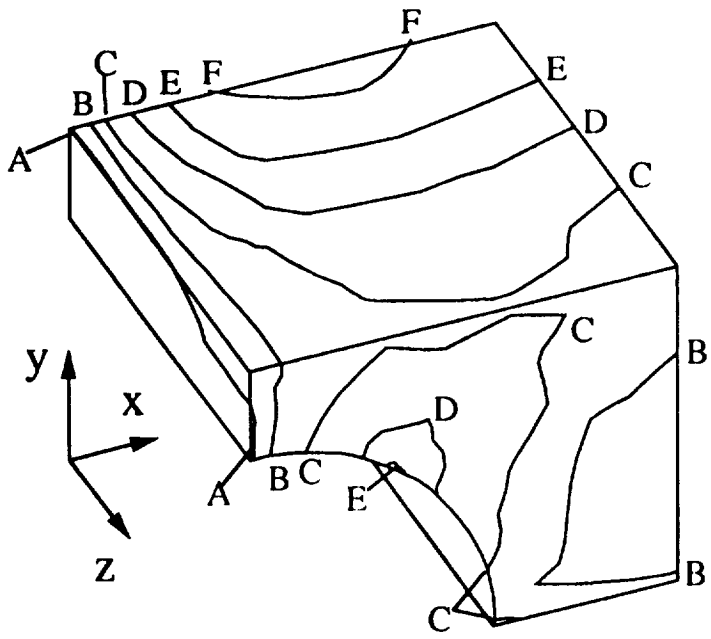

(a)

Level	Stress (MPa)
A	14.5
B	-3.18
C	-20.8
D	-38.4
E	-56.1
F	-73.7
G	-91.4
H	-109

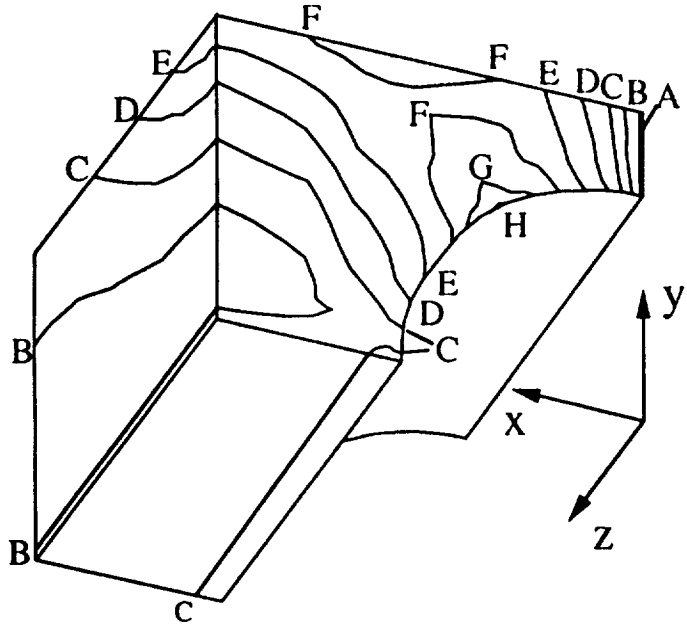

(b)

Figure 10. - Matrix $\tau_{r\theta}$ stress contours for [0/90] SCS-6/Ti-15-3, v_f = 32.5%, ΔT = -538°C.

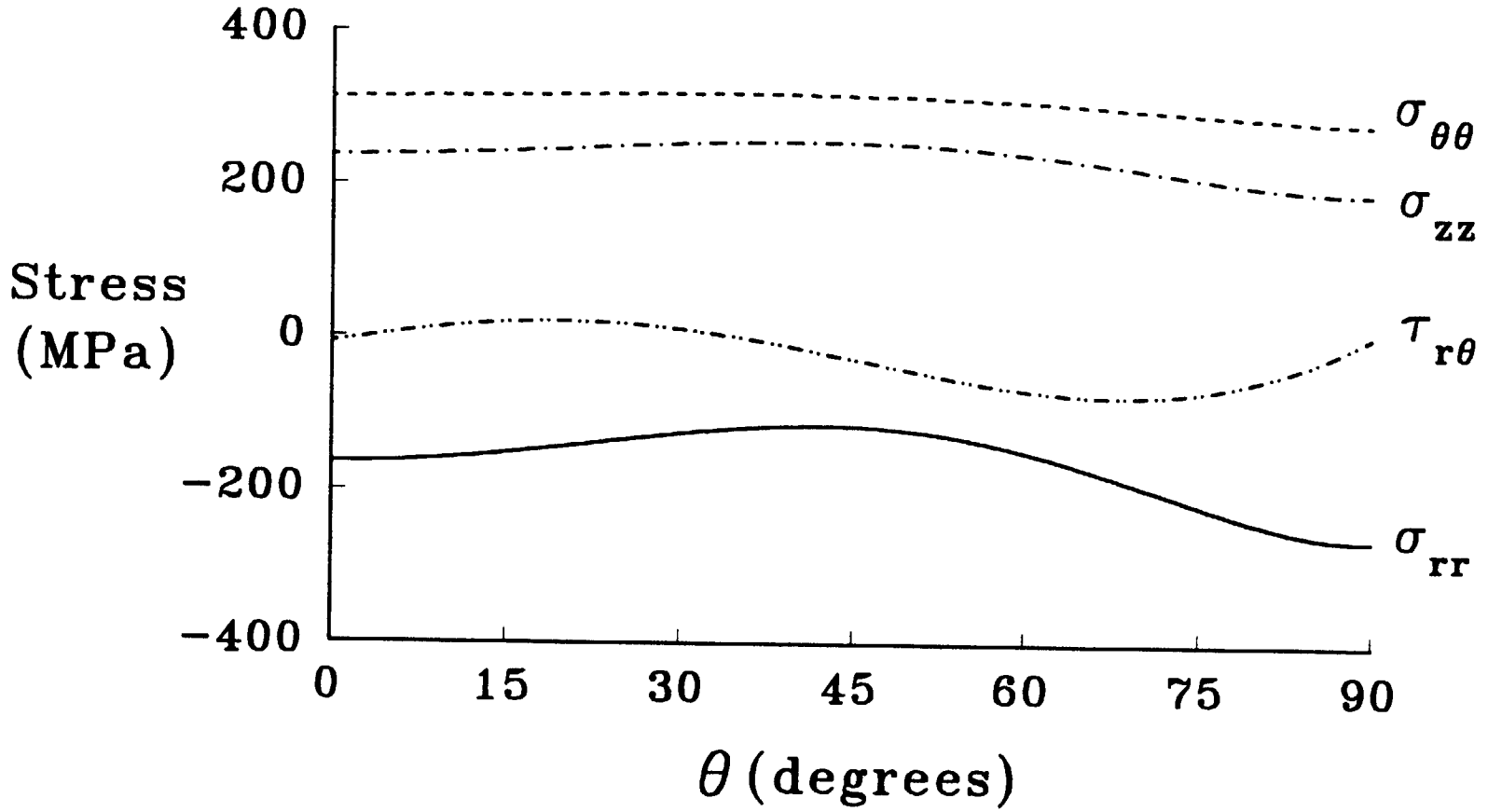

Figure 11 - Matrix interface stresses for the unidirectional SCS-6/Ti-15-3, v_f = 32.5%, ΔT = -538°C.

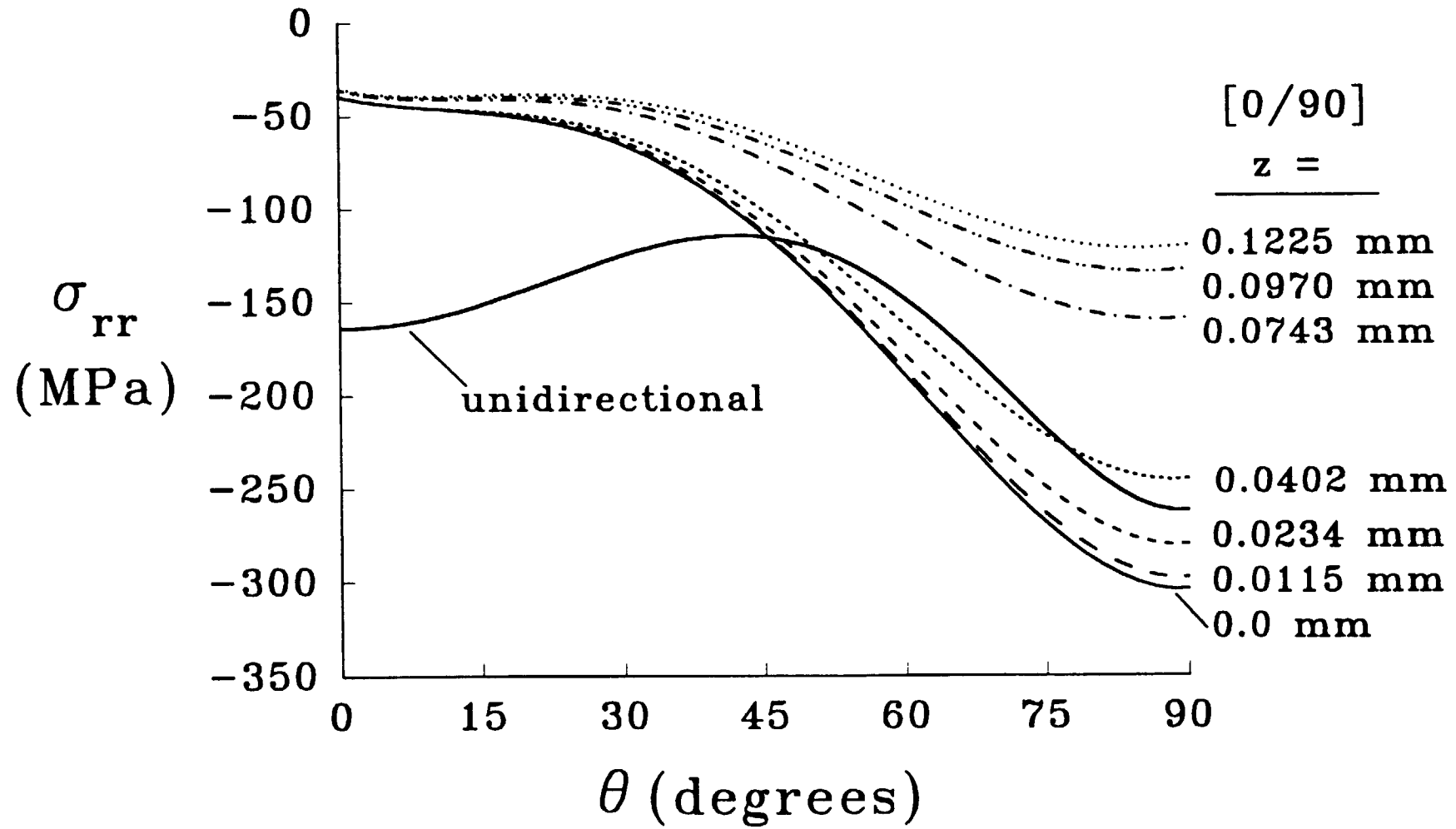
0
−50
−100
−150
−200
−250
−300
−350
σ_{rr} (MPa)
0
15
30
45
60
75
90
θ (degrees)
[0/90]
z =
0.1225 mm
0.0970 mm
0.0743 mm
0.0402 mm
0.0234 mm
0.0115 mm
0.0 mm
unidirectional

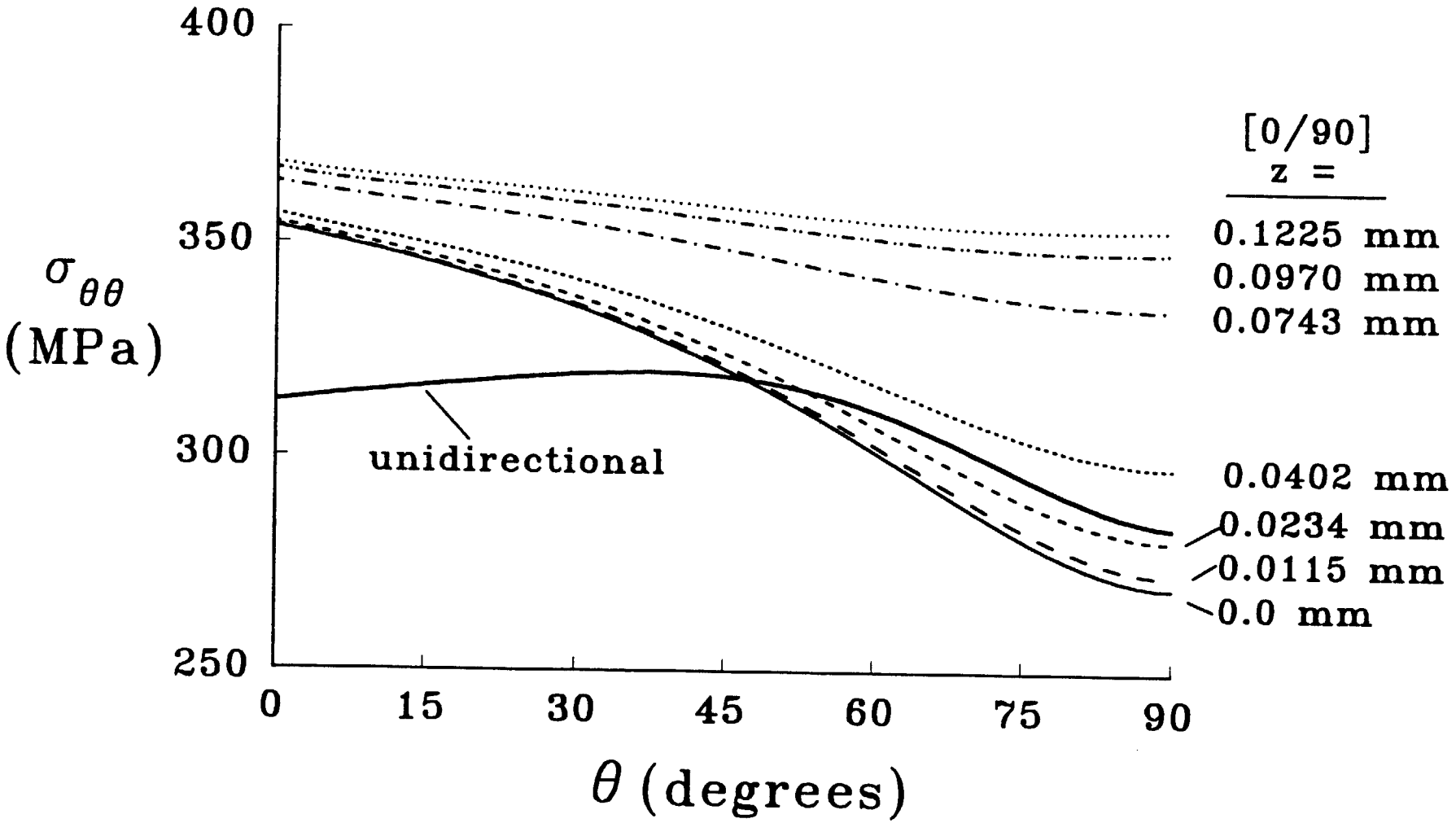

Figure 13 - Matrix $\sigma_{\theta\theta}$ interface stresses for the [0/90] SCS-6/Ti-15-3, v_f = 32.5%, ΔT = -538°C.

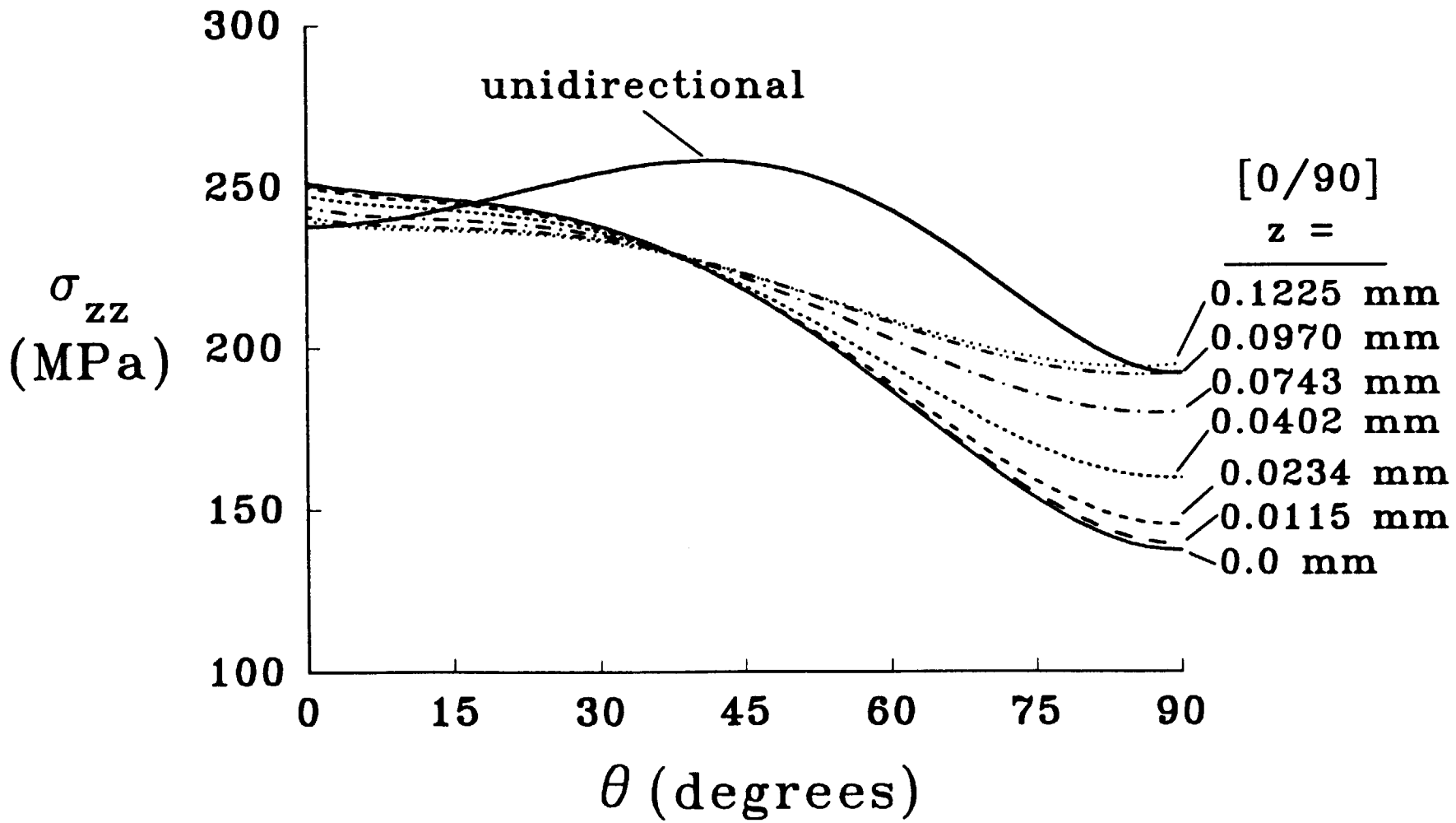

Figure 14 - Matrix σ_{zz} interface stresses for the [0/90] SCS-6/Ti-15-3, v_f = 32.5%, ΔT = -538°C.

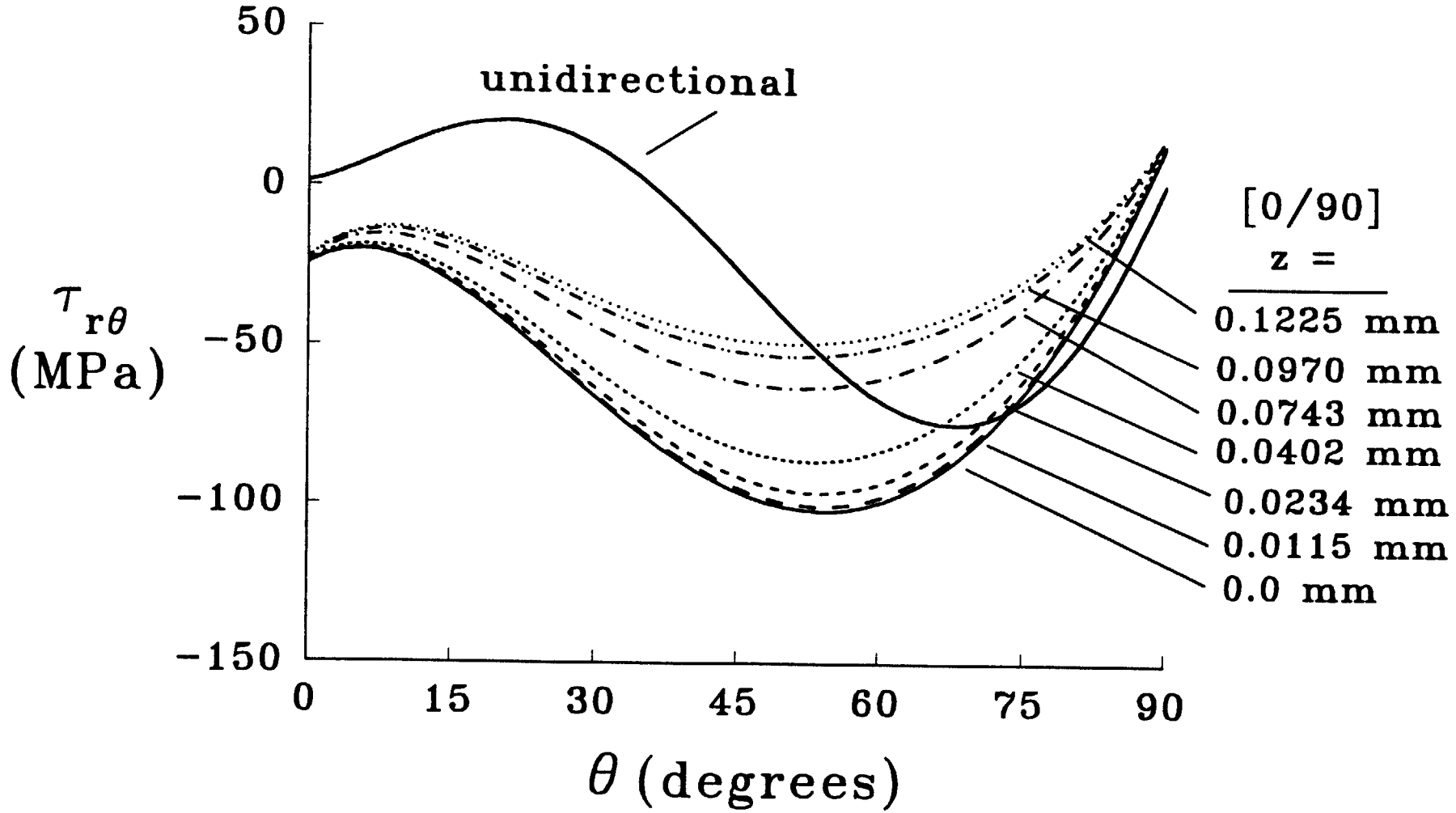

Figure 15 - Matrix $\tau_{r\theta}$ interface stresses for the [0/90] SCS-6/Ti-15-3, v_f = 32.5%, ΔT = -538°C.

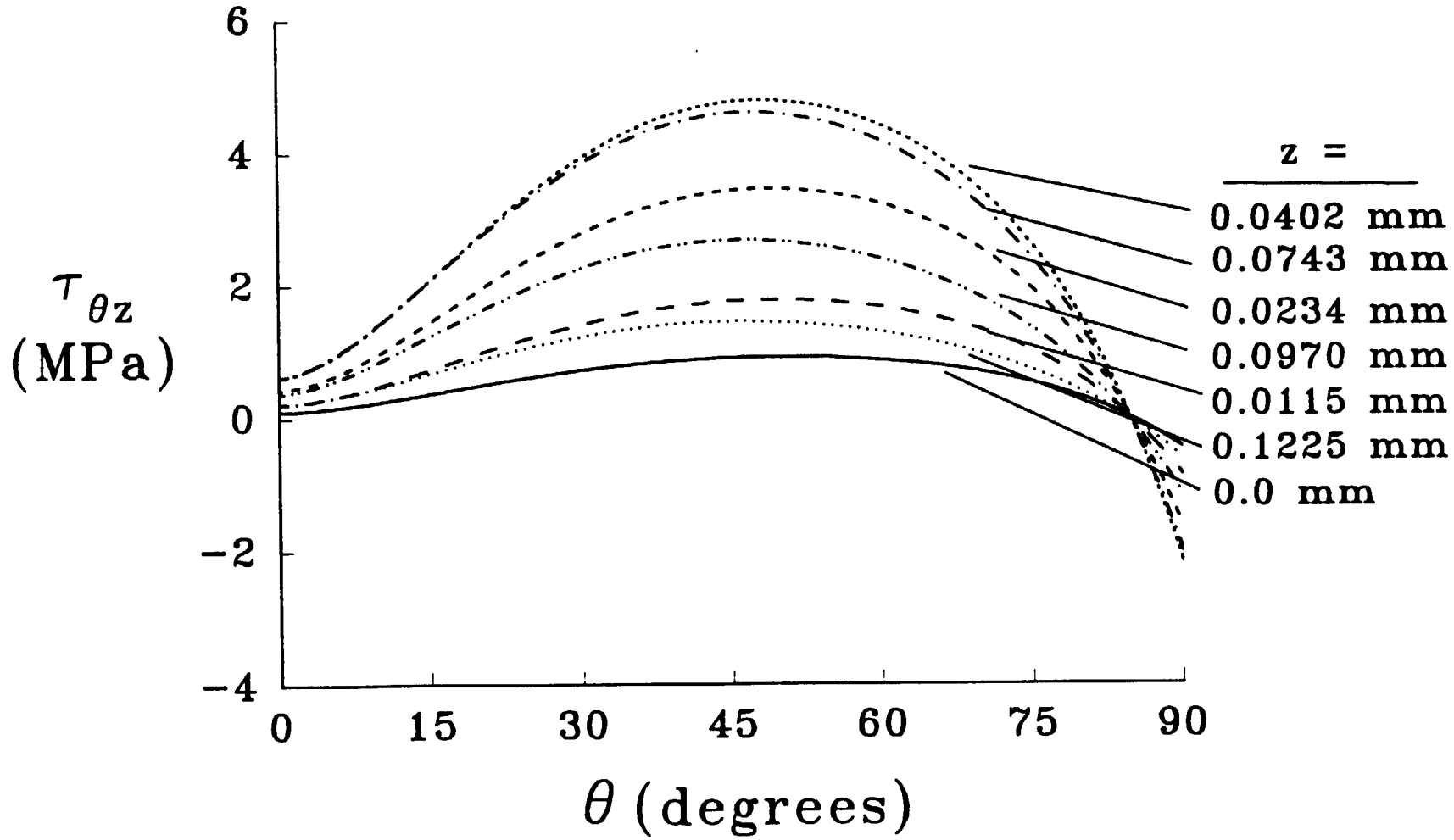

Figure 16 - Matrix $\tau_{\theta z}$ interface stresses for the [0/90] SCS-6/Ti-15-3, v_f = 32.5%, ΔT = -538°C.

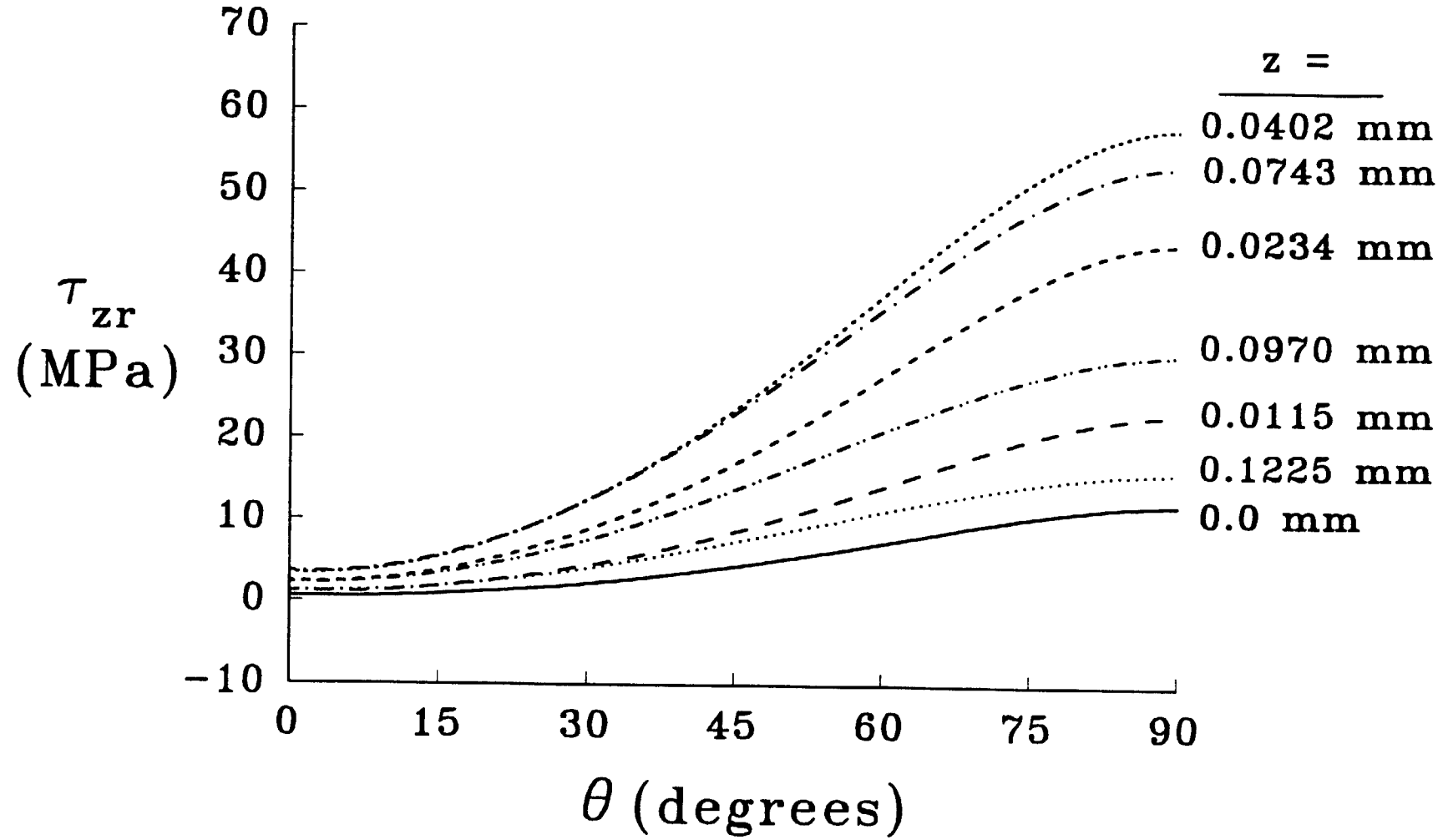

Figure 17 - Matrix τ_{zr} interface stresses for the [0/90] SCS-6/Ti-15-3, v_f = 32.5%, ΔT = -538°C.

REPORT DOCUMENTATION PAGE

Form Approved
OMB No. 0704-0188

1. AGENCY USE ONLY *(Leave blank)*	2. REPORT DATE	3. REPORT TYPE AND DATES COVERED
	July 1992	Technical Memorandum

4. TITLE AND SUBTITLE

Thermal Residual Stresses in Silicon-Carbide/Titanium [0/90] Laminate

5. FUNDING NUMBERS

WU 763-23-41-85

6. AUTHOR(S)

C. A. Bigelow

7. PERFORMING ORGANIZATION NAME(S) AND ADDRESS(ES)

NASA Langley Research Center
Hampton, VA 23665-5225

8. PERFORMING ORGANIZATION REPORT NUMBER

9. SPONSORING/MONITORING AGENCY NAME(S) AND ADDRESS(ES)

National Aeronautics and Space Administration
Washington, DC 20546

10. SPONSORING/MONITORING AGENCY REPORT NUMBER

NASA TM-107649

11. SUPPLEMENTARY NOTES

12a. DISTRIBUTION/AVAILABILITY STATEMENT

Unclassified - Unlimited

Subject Category - 24

12b. DISTRIBUTION CODE

13. ABSTRACT *(Maximum 200 words)*

The current work formulated a micromechanical analysis of a cross-ply laminate and calculated the thermal residual stresses in a very thick $[0/90]_{2n}$ silicon-carbide/titanium laminate. Results were also shown for a unidirectional laminate of the same material. Discrete fiber-matrix models assuming a rectangular array of fibers with a fiber volume fraction of 32.5% and a three-dimensional, finite-element analysis were used. Significant differences in the trends and magnitudes for the fiber, matrix, and interface stresses were calculated for the unidirectional and [0/90] models. Larger hoop stresses calculated for the [0/90] model indicate that it may be more susceptible to radial cracking when subjected to mechanical loading than the unidirectional model. The axial stresses in the matrix were calculated to be slightly larger for the [0/90] model. The compressive axial stresses in the fiber were significantly larger in the [0/90] model. The presence of the cross-ply in the [0/90] model reduced the constraint on the fiber, producing radial interface stresses that were less compressive, which could lead to earlier failure of the fiber-matrix interface.

14. SUBJECT TERMS

Cross ply; Unidirectional;Finite element analysis
Micromechanics; Stress contours

15. NUMBER OF PAGES

27

16. PRICE CODE

A03

17. SECURITY CLASSIFICATION OF REPORT	18. SECURITY CLASSIFICATION OF THIS PAGE	19. SECURITY CLASSIFICATION OF ABSTRACT	20. LIMITATION OF ABSTRACT
Unclassified	Unclassified		